Journal of Photochemistry and Photobiology A: Chemistry 218 (2011) 213–218

Contents lists available at ScienceDirect

Journal of Photochemistry and Photobiology A: Chemistry

journal homepage: www.elsevier.com/locate/jphotochem

Microdynamics behavior of the photogenerated carriers in ligand-capped CdTe quantum dots

Kuiying Li*, Guangjing Song, Jian Zhang, Chunmei Wang, Bin Guo

State Key Laboratory of Metastable Materials Manufacture Technology & Science, Yanshan University, Qinhuangdao 066004, China

ARTICLE INFO

Article history:
Received 3 October 2010
Received in revised form 3 January 2011
Accepted 4 January 2011
Available online 6 January 2011

Keywords:
Capping ligand CdTe
Quantum dot
Transient photovoltaic spectroscopy
Surface photovoltaic spectroscopy
Photoacoustic spectroscopy

ABSTRACT

A microdynamics study of high-quality CdTe/ligand self-assembled quantum dots (QDs) is significant because it is closely related to the energy transformation among specific quantum states, such as the electron and vibration levels of an elementary reaction. Transient photovoltaic (TPV) technology was used to probe the microdynamics behavior of the photogenerated carriers in the QDs. The TPV polarity of the nanocrystalline CdTe particles depended on the type of capping ligand used [3-mercaptopropionic acid (MPA) or β-mercaptoethylamine (MA)] because of a quantum tunneling effect. This resulted in a negative TPV polarity of the MPA samples upon illumination with a laser pulse of 532 nm and excitation intensity of 50 μJ, the opposite to the situation for the MA sample. The effect of the concentration of Cd^{2+} cations on the separation and recombination rates of the photo-induced free charge carriers of the CdTe/MPA self-assembled QDs was negligible. The different chemical bonds that formed at the interface between the core-CdTe nanoparticles and the capping ligand led to the change in the intensity of the photoacoustic signal in the 550–800 nm region caused by the non-radiative de-excitations as compared to the CdTe QDs capped by MA with that capped by MPA, and to the differences in the Raman scattering between the two samples. The property of those lattice vibration quantum states locating at the Brillouin zone boundary or near the Brillouin zone boundary was associated to a great extent with the formation of the shell-CdS in between the core-CdTe and the capping ligand according to the computer simulation results.

1. Introduction

The semiconductor nanocrystals known as quantum dots (QDs) have aroused great interest in theoretical research and experimental work in the fields of optical, electrical and magnetic materials, because of their quantum confinement effects [1–4]. One particular high-quality QD consisting of II/VI semiconductors, a core–shell structural nanocrystalline CdTe capped by various ligands, has the potential for widespread use in the fields of biomarkers, luminescent materials, and photon crystals [5–7]. In the past decade, research into the characteristics of CdTe/ligand self-assembled QDs, such as their photoluminescence and microstructure, and into their use in hetero-junctions, [8–11], has been steadily on the increase. In terms of the methods used to research this material, surface photovoltaic technology has been less utilized than methods such as luminescent spectroscopy and absorption spectrometry, even though it is a very efficient tool for probing the surface electron structure and photoexcited charge transfer (CT) transition behavior at surfaces and grain boundaries of semiconductor nanocrystalline particles [12,13]. In our previous study [14], the mechanism of charge transport in CdTe QDs capped by a ligand of 3-mercaptopropionic acid (MPA) or β-mercaptoethylamine (MA), was probed by a combination of surface photovoltaic (SPV) and photoacoustic (PA) techniques, in which it was directly experimentally confirmed that a layer of $CdTe_{1-x}S_x$ ($0 < x \leq 1$) formed at the interface in between the nanocrystalline CdTe particles and the ligand. However, steady-state photovoltage spectroscopy cannot directly probe the microdynamics of the photoinduced carriers which is vital to interpret the systemic macrodynamic phenomena. As is well known, the study of microdynamics for semiconductor nanocrystals is closely related to the energy transformation among specific quantum states, such as the electron and vibration levels of an elementary reaction. But some low-frequency technologies (generally at 10–1000 Hz), for example, impedance spectroscopy and light-current spectrum, only provide information on the microscopic processes relating to the time and space averages of macro-parameters [15,16]. Fortunately, the transient photovoltage (TPV) technique can directly provide information about photoinduced charge separation dynamics [17–20]. And the specific quantum states of the ligand-capped CdTe QDs may be associated with both CT transition behaviors of photon excitation and lattice vibrations caused by photoelectron non-radiative de-

* Corresponding author. Tel.: +86 335 8074631; fax: +86 335 8057047.
E-mail address: kuiyingli@ysu.edu.cn (K. Li).

1010-6030/$ – see front matter © 2011 Elsevier B.V. All rights reserved.
doi:10.1016/j.jphotochem.2011.01.001

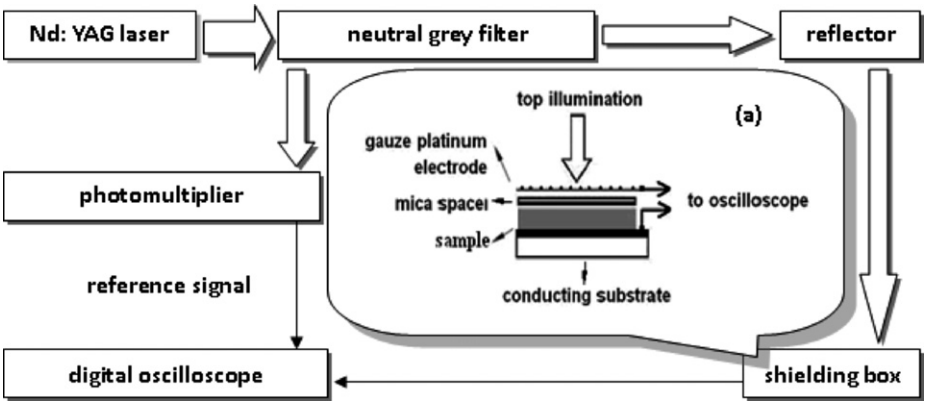

Scheme 1. Home-built set-up for transient photovoltaic spectroscopy. Thick hollow arrow indicates the primary laser; the thin hollow arrows indicate the attenuated laser; and the thin solid arrows represent cable connections; details of the sample cell (a) are also included.

excitation processes, especially by means of the combination of photovoltaic and photoacoustic technologies. However, this has seldom been reported so far. In the present paper, we focus attention on probing the CT transition microdynamics of CdTe/ligand self-assembled QDs, according to the results of TPV measurements, supplemented by SPV, PA, and laser Raman spectra, and by a computer simulation method using the CASTEP module in the materials studio software.

2. Experimental

2.1. Sample preparation

CdTe nanocrystals were prepared according a previously published method of aqueous synthesis at room temperature [21,22]. Briefly, freshly prepared NaHTe solution was injected into a solution of $CdCl_2$ and MPA or MA which was degassed with N_2 for 30 min at pH 9.5. The concentration of $CdCl_2$ was 1.25×10^{-3} mol/L and the Cd^{2+}/MPA (or MA)/Te^{2-} molar ratio was 1:2.4:0.2. The crude solution was refluxed at 100 °C for 10 h to obtain CdTe nanocrystals. The number of CdTe nanocrystals in solution was calculated as 10^{-5} to 10^{-6} mol/L.

The samples prepared were denoted as MPA-r, MPA-l, and MA-r, where MPA-r indicated MPA-capped CdTe nanoparticles with an average particle size of 4.0 nm (red) at a Cd^{2+} concentration of 0.01 M; MPA-l denoted the sample prepared at a lower Cd^{2+} concentration (0.001 M); MA-r was MA-capped CdTe nanoparticles with an average particle size of 4.0 nm (red) at a Cd^{2+} concentration of 0.01 M.

The X-ray diffraction (XRD) pattern was obtained using a Rigaku D/Max-2500/PC X-ray diffractometer with Cu K_α radiation. The microstructure and component were determined by a confocal Raman microscope (inVia, England). All optical measurements were performed at room temperature under ambient conditions.

2.2. TPV, SPV, and PA spectroscopy

Scheme 1 shows the TPV testing equipment diagram and detailed structure of the sample cell. The light source was a YAG:Nd pulse laser (Polaris II, New Wave Research, Inc. USA);, the pulse half-width was 5 ns, and the base frequency 1064 nm was converted by a frequency-doubling crystal to a 532 nm laser beam. In the testing process, the intensity of the laser light could be adjusted by a gradient circular neutral density filter. The attenuated laser illuminated the sample cell. Scheme 1a illustrates that the platinum network in the cell allowed it to play the role of the electrode, while allowing the light through. The wafer-thin mica sheet was placed between the platinum network and the sample. Another electrode was a transparent conductive indium tin oxide glass.

The setup diagram and the principle of steady-state SPV and PA spectroscopy were described in detail elsewhere [23,24]. In our experiment the detection device and the conditions of the two tests, with illumination by ultraviolet-near infrared (UV–NIR) light, were the same except for exchanging the sample cells. The resulting PA spectra of the samples were normalized using the spectrum of carbon black. SPV and PA technologies can also be used effectively to get information about photoelectron behaviors at interfaces, because the techniques are by no means sensitive only to surfaces. Rather, they are sensitive to the entire surface space charge region (SCR) by super- or sub-bandgap absorption, even to buried interfaces located anywhere in the sample, as long as they can be reached by photons [23].

3. Results and discussion

3.1. Microstructure of the samples

Fig. 1a shows XRD pattern of the prepared CdTe nanocrystal capped by MPA. According to the Scherrer formulae the average particle size of the sample was about 3 nm; the three peaks that located at 24.42°, 40.82°, and 47.76° in Fig. 1a corresponded to plans (1 1 1), (2 2 0), and (3 1 1), respectively; in contrast to the Standard Spectra JCPDS 15-0770 these peaks were intermediate between that of CdTe and CdS, but were shifted to be more of CdTe than CdS. The results above imply that small quantities of CdS were formed on CdTe nanoparticles. Furthermore, a distortion of the lattice cell occurred because S atoms in ligand MPA partially replaced Te atoms that located at the surfaces and the boundary of CdTe nanoparticles, as illustrated in Fig. 1b.

3.2. Analysis of TPV spectroscopy

Fig. 2 displays the TPV spectra of the samples MPA-r, MPA-l, and MA-r. The difference in the TPV responses between the samples MA-r and MPA-r is as follows. First, the polarity of the TPV response of the sample MA-r was positive, whereas that of the sample MPA-r was negative. Second, the range of the TPV response of the sample MA-r was broader than that of the sample MPA-r. Third, the extrema of the TPV response of MA-r and MPA-r appeared at 2.3×10^{-6} s and 2.2×10^{-7} s, respectively. In addition, the TPV characteristic of the sample MPA-l was very similar to that of the sample MPA-r as seen in Fig. 2.

The results mentioned above show that the TPV polarity was closely dependent on the type of ligand that capped the nanocrys-

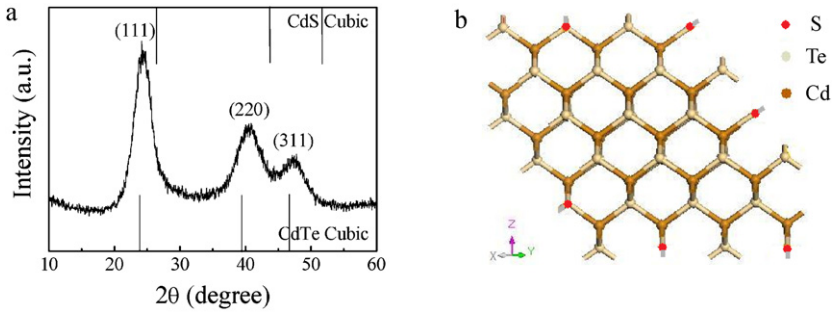

Fig. 1. XRD pattern of the sample MPA-r (a); the skeleton map of the plane (1 1 1) of $CdTe_{1-x}S_x$ ($0 < x \leq 1$) (b), in which another bond of S may be bonded to a carboxylic acid group.

talline CdTe particles. Specifically, the sample MA-r displayed an n-type TPV characteristic because of its positive TPV response upon illumination by excitation wavelength of 532 nm and intensity 50 μJ, while the sample MPA-r exhibited a p-type TPV characteristic because of its negative TPV response upon being illuminated by the same laser pulse according to the literature [25]. This is in good agreement with the results of the electric field-induced SPV spectra of the two samples [14]. Our previous work [14] established that another transport tunnel for photoexcited free charge carriers (FCCs) was existed between the ligand and the nanocrystalline CdTe particles, apart from the normal charge transport tunnel of the photo-induced FCCs. The former was related to the quantum tunnel effect, and the direction of electronic movement in the tunnel was opposite to that of the latter. Consequently, the overall direction of movement of the photo-generated FCCs should result from the combined influence of the build-in field and the quantum tunnel effect of the material. This model is strongly supported by the p-type TPV characteristic of the sample MPA-r at 532 nm laser pulse and 50 μJ excitation intensity. In other words, the MPA-capped nano-CdTe possessed a more obvious quantum tunnel effect as compared to the MA-capped nano-CdTe, which is responsible for the negative transient PV polarity of the sample MPA-r in Fig. 2.

According to Ref. [17] the extent of the TPV response depends on the proportion of the thickness of SCR to the length of the FCCs drift in SCR, and/or on the diffusion distance of electron–hole pairs. Therefore, it is supposed that the rapid decay of the TPV response of the samples MPA-r in Fig. 2 may be attributed to the fact that the length of the FCCs drift was equal to the thickness of surface (or interface) SCR, while the slow decay of the TPV response of the sample MA-r in Fig. 2 may result from the thickness being larger than the length. More specifically, the thickness of the interface SCR_1 between the core-CdTe and the CdS layer of the ligand MA-capped CdTe nanoparticles was larger than that of the ligand MPA-capped CdTe nanoparticles because of the difference in the chemical bond formed between the ligand and nano-CdTe. This is confirmed by the results of the SPV, PA, and laser Raman spectra of these samples, and by the computer simulation using the CASTEP method for $CdTe_{1-x}S_x$ ($0 < x \leq 1$) below.

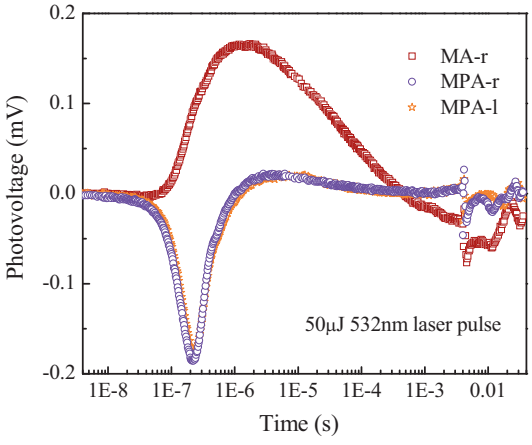

Fig. 2. Transient photovoltage spectra of the samples MA-r, MPA-r, and MPA-l.

In a normal situation the separation rate of the photo-induced FCCs is faster than their recombination rate before achieving the extrema of TPV responses. By contrast, the recombination rate is faster than the separation rate after the extrema according to Refs. [17,26]. As mentioned above, the extremum of the TPV response of the sample MA-r was located at 2.3×10^{-6} s, which was about an order of magnitude greater than that of the sample MPA-r, as seen in Fig. 2. This implies that in the nanocrystalline CdTe particles capped by the ligand MPA it was easier to produce the electron–hole pair as compared with the sample capped by the ligand MA upon photoinduction by the 532 nm laser pulse (50 μJ). And the recombination rate of the electron–hole pair of the former was faster than that of the latter, resulting in the intensity of the TPV responses of the former rapidly decaying in the region 2.9×10^{-8} to 1.6×10^{-6} s, while that of the latter slowly decayed in the region 7.0×10^{-8} to 5.7×10^{-4}s (Fig. 2). In addition, a plateau in the TPV responses of the latter appeared in the region 7.7×10^{-7} to 2.6×10^{-6} s in Fig. 2, in which the separation rate of the FCCs was equal to their recombination rate. In addition, the comparison of the TPV spectra of the samples MPA-r and MPA-l reveals that the effect of the concentration of the Cd^{2+} cations on the separation and recombination rates of the photo-induced FCCs upon illumination by a 532 nm laser pulse may be negligible because of the uniform TPV that is characteristic of them in Fig. 2, which was distinct from the effect of the concentration on the SPV characteristic of the samples in Fig. 3.

3.3. *Analyses of SPV, PA, and laser Raman spectra*

According to the literature [14,27], the shape of the SPV spectrum resembles a typical (inverted) absorption spectra of the multiple quantum-well (QW) structure as per QW_1 and QW_2 indicated in Fig. 3, in which knee 1, knee 2, and knee 3 correspond to the SPV responses of the core CdTe, the shell CdS, and the capping ligand, respectively; QW_1 and QW_2 were located at the interface SCR_1 between the core CdTe and the shell CdS, and at the interface SCR_2 between the shell CdS and the capped ligand, respectively. Furthermore, it may be supposed that the structures of the QW_1 and QW_2 obviously affected the transport behavior of the photo-generated FCCs at the buried interfaces SCR_1 and SCR_2 upon illumination with UV–NIR light. As seen in Fig. 3 the SPV responses of the sample MA-r at the wavelength region of 300–700 nm were obviously higher

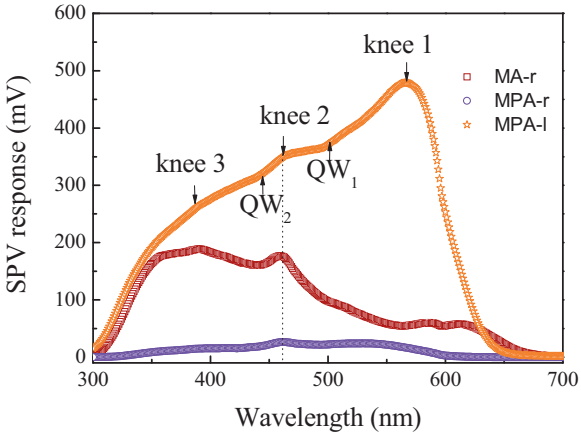

Fig. 3. Surface photovoltage spectra of the samples MA-r, MPA-r, and MPA-l. 'knee 1', 'knee 2', and 'knee 3', and the quantum wells QW_1 and QW_2 are explained in the text.

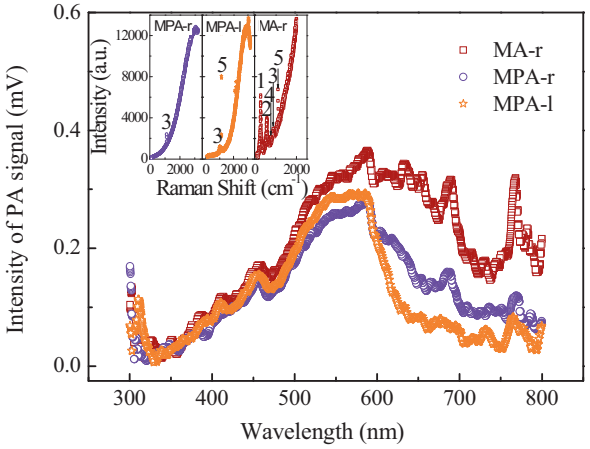

Fig. 4. Photoacoustic spectra of the samples MA-r, MPA-r, and MPA-l; the inset shows the laser Raman spectra of the three samples, in which the meaning of numerals 1–5 are explained in the text.

than that of the sample MPA-r, and the order of the intensity of the SPV response, *I*, of the former was $I_{knee1} > I_{knee2} > I_{knee3}$ which was opposite to that of the latter. This reveals that the minority carrier lifetime of the sample MA-r upon illumination by UV–NIR light was longer as compared with the sample MPA-r, which is in good agreement with their TPV results in Fig. 2. On the other hand, the intensity of the SPV response of the samples MPA-l in the 350–630 nm region dramatically increased as compared with the sample MPA-r, as shown in Fig. 3, due to the concentration of Cd^{2+} cations of the sample MPA-l being 10 times more dilute than that of the sample MPA-r. This was very different from the situation of the TPV responses of the two samples in Fig. 2. Consequently, this demonstrates that the concentration of Cd^{2+} cations played an important role in the steady-state SPV responses of the nano-CdTe, quite unlike the situation of the TPV spectrum of these samples in Fig. 2. In other words, the effect of the concentration of Cd^{2+} cations on the TPV characteristic of the nano-CdTe capped by the ligand MPA can be neglected, but it is a factor that cannot be ignored with respect to its SPV characteristic. Furthermore, to reduce the concentration of the Cd^{2+} cations may obviously reduce the surface/interface potential barrier of the CdTe/MPA self-assembled QDs, resulting in a strong SPV response of the sample MPA-l in the 350–630 nm region in Fig. 3. However, there was no difference between the TPV responses of the samples MPA-r and MPA-l because they were identical in the structure of their CdS layers in between the core-CdTe and the ligand MPA. And this was confirmed by the SPV responses of the knee 2 having the same peak positions, at the wavelength of 461 nm in Fig. 3, for the samples MPA-r and MPA-l.

To probe the lattice vibrations causing by non-radiative energy transformation in the de-excitation process when illuminated by UV–NIR light, Fig. 4 shows the PA spectra of the samples MA-r, MPA-r, and MPA-l. The profiles of the PA spectra of the three samples were basically the same, i.e. strong PA signals appeared at 450 nm, the 550–650 nm region, and 780 nm, respectively, and most PA signals were located in the 550–650 nm region and the wavelength of 780 nm in Fig. 4. These findings imply that the energy released from the non-radiative de-excitation processes was close to but less than the bandgaps of CdTe ($E_{g,\ core\text{-}CdTe}$ = 1.58 eV) and CdS ($E_{g,\ shell\text{-}CdS}$ = 2.48 eV), respectively. Furthermore, the initial energies of the non-radiative de-excitation processes were mostly concentrated either near or lower than the bottom of the conduction band (i.e. at the Brillouin zone boundary or near the Brillouin zone boundary) of the shell-CdS because of the quantum tunnel effect. That is, apart from partially appearing at near or below the bottom of the conduction band of the core-CdTe, which resulted in the strong PA signals in the 550–650 nm region and the wavelength of 780 nm. The differences in the PA spectra among the three samples were located at these regions (Fig. 4). More specifically, the order of the intensity of the PA signals, *I*′, was $I_{MA\text{-}r}' > I_{MPA\text{-}r}' > I_{MPA\text{-}l}'$ for the three samples in the 550–800 nm region. This reveals that the lattice vibration causing by non-radiative de-excitation of the sample MA-r in the region 550–800 nm was obviously stronger than that of the samples MPA-r because of the differences in the chemical bond formation between nanocrystalline CdTe particle and the ligand [28]. In addition, the difference in the PA signal intensity between the samples MPA-r and MPA-l confirms that reducing the concentration of Cd^{2+} cations may reduce the probability of the non-radiative de-excitation process appearing. Combining the results of the SPV spectra in Fig. 3 and the PA spectra in Fig. 4 in terms of the samples MPA-r and MPA-l, further confirms the complementary relationship of energy conversion between photoacoustic and photovoltaic effects.

Other lattice vibration quantum states might appear in the laser Raman spectrum in the inset in Fig. 4. The sample MA-r displayed many more Raman scattering peaks of various lattice vibration patterns as compared with the MPA-r and MPA-l samples. According to Refs. [29,30], these were 1LO (301 cm^{-1}), 2LO (603 cm^{-1}), 3LO (908 cm^{-1}), CSA (1100 cm^{-1}), and S-peak (895 cm^{-1}), respectively, in which 1LO, 2LO, and 3LO represent the first, second, and third order longitudinal optical phonon pattern of CdS, respectively, and belong to the molecular and interionic optical vibration patterns; CSA was related to the absorption behavior of the carbon skeleton of the ligand; and the S-peak induced by the laser beam in the testing procedure was produced by splitting CdS into its elements. For the sample MPA-r, however, there was only a peak resulting from the CSA vibration pattern at the same testing condition. The results above verify that the different ligand might cause distinct chemical bonds between the core-CdTe and the MPA or MA ligand and be responsible for the varied surface/interface electron structures of the samples MPA-r and MA-r corresponding to the results in Fig. 3. It is more notable that the vibration patterns mentioned above could lead to a micro-scale deformation in the lattice cell despite the fact that they do not cause a macro-scale deformation of the samples as displayed in the XRD pattern of the sample MPA-r in Fig. 1a. Consequently, the Raman scattering of the semiconductor nanocrystal was related to a great extent to the interaction of the electrons (in the photo-induced FCCs) and phonons (located at the Brillouin zone boundary or near the Brillouin zone boundary, i.e. the bottom of the conduction band or the top of the valence band), according to Ref.

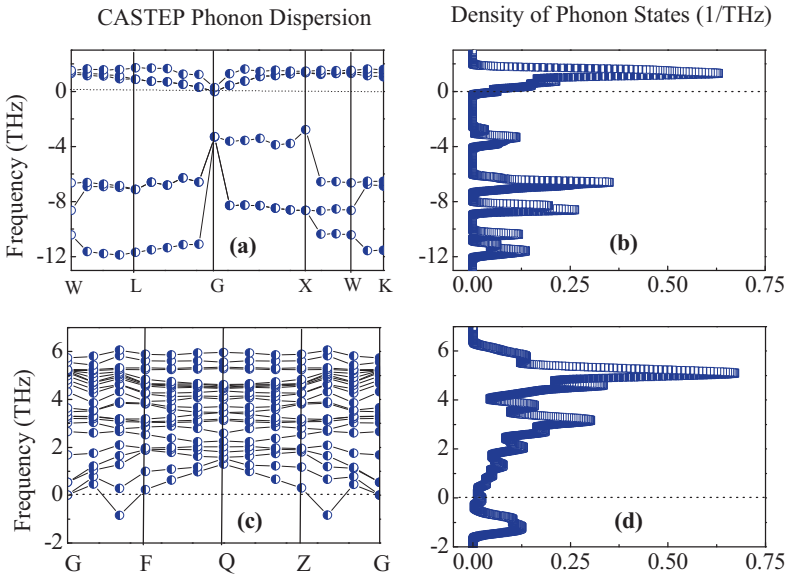

Fig. 5. Phonon spectra of CdTe and $CdTe_{1-x}S_x$ ($x = 0.5$) calculated by the CASTEP method, in which (a) and (b) display the phonon dispersion curves and the density of phonon states of crystalline CdTe, respectively; (c) and (d) are the phonon dispersion curves and the density of phonon states of crystalline $CdTe_{1-x}S_x$ ($x = 0.5$), respectively.

[31]. The shell-CdS in between nano-CdTe and the ligand may be too valuable to be neglected in the electron–phonon interaction of the material as the computer simulation result by CASTEP module below demonstrates.

3.4. CASTEP simulation results

Fig. 5 shows the phonon spectra of both CdTe that belongs to the space group F−43M and $CdTe_{1-x}S_x$ ($x = 0.5$) as obtained by the CASTEP computer simulation method. The phonon dispersions of CdTe with sphalerite structure show six dispersion curves, i.e. six kinds of phonon vibration patterns in Fig. 5a, in which three dispersion curves possessed the longitudinal acoustic (LA) mode characteristic that has a maximum frequency at the edge of the Brillouin zone and a minimum frequency equal to zero at the center of the Brillouin zone, G, and the other three curves possessed the longitudinal optical (LO) mode characteristic that has a maximum frequency at the center of the Brillouin zone, and a minimum frequency at the edge of the Brillouin zone according to Ref. [32]. The vibration quantum state was in a metastable state when the frequency of the phonon dispersions was smaller than zero [33]. The density of phonon states of CdTe in Fig. 5b corresponded to these phonon dispersions in Fig. 5a, in which the density of LO mode phonon states was greater than that of the LA mode phonon states. And the state of the former was more stable than that of the latter. The PA spectra of the samples MPA-r, MPA-l, and MA-r at 780 nm in Fig. 3 might correspond to the simulation results. It is more notable that 24 phonon dispersion curves appeared in the phonon spectrum of $CdTe_{1-x}S_x$ ($x = 0.5$) in Fig. 5c. They are more stable than that of the pure CdTe because almost all vibration frequencies were greater than zero, as shown in Fig. 5d. This demonstrates that many more phonons should be produced after a lot of S is doped into CdTe. These lattice vibration quantum states were dependent on those new chemical bonds resulting from doping S, which were responsible to a great extent for the strong PA signals of the samples MPA-r, MPA-l, and MA-r in the 550–650 nm region in Fig. 4 and the vibration consisting of patterns 1LO, 2LO, 3LO and S-peak of Raman scattering in Fig. 4 inset. Consequently, it is supposed that the pattern of the vibration quantum states of the CdTe/ligand self-assembled QDs may vary when employing different ligands. In other words, the property of the localized phonons depends on the type of the ligand, resulting in the differences in both the PA spectra at 550–650 nm and the Raman spectra among the three samples.

4. Conclusions

In summary, the microdynamics behavior of the photogenerated carriers in CdTe/ligand self-assembled QDs may be probed using TPV measurements supplemented by surface photovoltaic, photoacoustic, and laser Raman spectra, and by a computer simulation method of the CASTEP module. Firstly, the results showed that the TPV polarity of the nanocrystalline CdTe particles capped by a ligand was strongly dependent on the type of the ligand. This was because of a quantum tunneling effect, resulting in a negative TPV polarity of the samples MPA-r and MPA-l possessing obvious quantum tunnel effect when excited by a laser pulse at 532 nm and 50 μJ pulse intensity, which was opposite to the situation for the sample MA-r. Secondly, the experiment reveals that the effect of the concentration of Cd^{2+} cations on the separation and recombination rates of the photo-induced FCCs and TPV polarity of the CdTe/MPA self-assembled QDs was negligible. This resulted in the same TPV responses of the samples MPA-r and MPA-l upon illumination by the laser pulse of 532 nm (50 μJ). But to reduce the concentration might dramatically reduce the surface/interface potential barrier and the probability of the non-radiative de-excitation process for the MPA-capped sample appearing. These led to a stronger surface photovoltaic response of the sample MPA-l in the 350–600 nm region upon illumination with UV–NIR light, and to a weaker PA signal of the sample in the region 550–650 nm upon illumination by UV–NIR light, as compared with the sample MPA-r. Finally, the facts that both the photoacoustic signals caused by the non-radiative de-excitations of the sample MA-r at the region of 550–800 nm were stronger than that of the sample MPA-r, and the difference of the Raman scattering between the two samples, were attributed to different chemical bonds forming at the interface between the core-CdTe nanoparticles and the capping ligand. More specifically, the properties of the lattice vibration quantum states located at the Brillouin zone boundary or near the Brillouin zone boundary were related to a great extent to the formation of the shell-CdS in between the core-CdTe and the capping ligand according to the computer simulation results.

Acknowledgments

We are grateful to NSFC (grant no. 20573090), Key Project of Natural Science Foundation of Hebei Provincial Department of Education (grant no. ZH200814). Prof. D.J. Wang is acknowledged for the technical assistance.

References

[1] M. Bruchez Jr., M. Moronne, P. Gin, S. Weiss, A.P. Alivisatos, Semiconductor nanocrystals as fluorescent biological labels, Science 281 (1998) 2013–2016.
[2] G.L. Tan, Q. Yang, U. Hömmerich, J.T. Seo, D. Temple, Linear and non-linear optical properties of capped CdTe nanocrystals prepared by mechanical alloying, Opt. Mater. 27 (2004) 579–584.
[3] F.W. Wise, Lead salt quantum dots: the limit of strong quantum confinement, Acc. Chem. Res. 33 (2000) 773–780.
[4] S. Kim, B. Fisher, H.-J. Eisler, M. Bawendi, Type-II quantum dots: CdTe/CdSe(core/shell) and CdSe/ZnTe(core/shell) heterostructures, J. Am. Chem. Soc. 125 (2003) 11466–11467.
[5] A.M. Smith, S. Dave, S. Nie, L. True, X. Gao, Multicolar quantum dots for molecular diagnostics of cancer, Expert Rev. Mol. Diagn. 6 (2006) 231–244.
[6] S.J. Cho, D. Maysinger, M. Jain, B. Röder, S. Hackbarth, F.M. Winnik, Long-term exposure to CdTe quantum dots causes functional impairments in live cells, Langmuir 23 (2007) 1974–1980.
[7] J.Y. Zhang, X.Y. Wang, M. Xiao, Modified spontaneous emission of CdTe quantum dots inside a photonic crystal, Opt. Lett. 28 (2003) 1430–1432.
[8] M.G. Mahesha, K.V. Bangera, G.K. Shivakumar, Characterization of p-CdTe/n-CdS hetero-junctions, Mater. Sci. Semicond. Process. 12 (2009) 89–93.
[9] Y. Zhang, Y. Li, X.P. Yan, Photoactivated CdTe/CdSe quantum dots as a near infrared fluorescent probe for detecting biothiols in biological fluids, Anal. Chem. 81 (2009) 5001–5007.
[10] H.S. Lee, H.L. Park, T.W. Kim, Formation mode of self-assembled CdTe quantum dots directly grown on GaAs substrates, J. Cryst. Growth 291 (2006) 442–447.
[11] W.-J. Kim, S.-J. Kim, K.-S. Lee, M. Samoc, A.N. Cartwright, P.N. Prasad, Robust microstructures using UV photopatternable semiconductor nanocrystals, Nano Lett. 8 (2008) 3262–3265.
[12] I. Mora-Sero, J. Bisquert, Th. Dittrich, A. Belaidi, A.S. Susha, A.L. Rogach, Photosensitization of TiO_2 layers with CdSe quantum dots: correlation between light absorption and photoinjection, J. Phys. Chem. C 111 (2007) 14889–14892.
[13] F. Streicher, S. Sadewasser, M.Ch. Lux-Steiner, Surface photovoltage spectroscopy in a Kelvin probe force microscope under ultrahigh vacuum, Rev. Sci. Instrum. 80 (2009), 013907-1–013907-6.
[14] K.Y. Li, H. Zhang, W.Y. Yang, S.L. Wei, D.Y. Wang, Mechanism of charge transport in ligand-capped crystalline CdTe nanoparticles according to surface photovoltaic and photoacoustic results, Mater. Chem. Phys. 123 (2010) 98–103.
[15] P.E. De Jongh, D. Vanmaekelbergh, Trap-limited electronic transport in assemblies of nanometer-size TiO_2 particles, Phys. Rev. Lett. 77 (1996) 3427–3430.
[16] J. Nelson, S.A. Haque, D.R. Klug, J.R. Durrant, Trap-limited recombination in dye-sensitized nanocrystalline metal oxide electrodes, Phys. Rev. B 63 (2001), 205321-1–205321-9.
[17] V. Duzhko, F. Koch, T.H. Dittrich, Transient photovoltage and dielectric relaxation time in porous silicon, J. Appl. Phys. 91 (2002) 9432–9434.
[18] D.C. Amm, F.W. Müller, G. Israel, Models for description of the influence of light intensity on the parameters of the transient photo-EMF of organic photoconductors, Phys. Chem. Chem. Phys. 3 (2001) 4096–4101.
[19] C.H. Lee, G. Yu, D. Moses, A.J. Heeger, V.I. Srdanov, Nonlinear transient photovoltaic response in Al/C_{60}/Au devices: control of polarity with optical bias, Appl. Phys. Lett. 65 (1994) 664–666.
[20] Th. Dittrich, Temperature dependent normal and anomalous electron diffusion in porous TiO_2 studied by transient surface photovoltage, Phys. Rev. B 73 (2006) 8, 045407-1–045407-8.
[21] H. Zhang, C.L. Wang, M.J. Li, X.L. Ji, J.H. Zhang, B. Yang, Fluorescent nanocrystal–polymer composites from aqueous nanocrystals: methods without ligand exchange, Chem. Mater. 17 (2005) 4783–4788.
[22] M.Y. Gao, S. Kirstein, H. Mühwald, A.L. Rogach, A. Komowski, A. Eychmüller, H. Weller, Strongly photoluminescent CdTe nanocrystals by proper surface modification, J. Phys. Chem. B 102 (1998) 8360–8363.
[23] L. Kronik, Y. Shapira, Surface photovoltage phenomena: theory, experiment, and applications, Surf. Sci. Rep. 37 (1999) 1–206.
[24] A. Rosencwaig, Photoacoustic spectroscopy of biological materials, Science 181 (1973) 657–658.
[25] B. Mahron, G. Boschloo, A. Hagfeldt, L. Dloczik, Th. Dittrich, Photovoltage study of charge injection from dye molecules into transparent hole and electron conductors, Appl. Phys. Lett. 84 (2004) 5455–5457.
[26] Q.L. Zhang, D.J. Wang, X. Wei, T.F. Xie, Z.H. Li, Y.H. Lin, M. Yang, A study of the interface and the related electronic properties in n-$Al_{0.35}Ga_{0.65}N$/GaN heterostructure, Thin Solid Films 491 (2005) 242–248.
[27] D. Gal, J. Beier, E. Moons, G. Hodes, D. Cahen, L. Kronik, L. Burstein, B. Mishori, M. Leibovitch, Y. Shapira, D. Hariskos, R. Klenk, H.W. Schock, Band diagram and band line-up of the polycrystalline CdS/Cu(In,Ga)Se_2 heterojunction and its response to air annealing, AIP Conf. Proc. 353 (1996) 453–462.
[28] H. Zhang, Z. Zhou, B. Yang, M.Y. Gao, The influence of carboxyl groups on the photoluminescence of mercaptocarboxylic acid-stabilized CdTe nanoparticles, J. Phys. Chem. B 107 (2003) 8–13.
[29] N. Romčević, M. Romčević, R. Kostić, D. Stojanović, B. Abolmasov, G. Karczewski, R. Galazka, Resonant Raman spectra of CdTe/ZnTe self assembled quantum dots, Acta. Phys. Pol. A 116 (2009) 88–90.
[30] A. Balandin, K.L. Wang, N. Kouklin, S. Bandyopadhyay, Raman spectroscopy of electrochemically self-assembled CdS quantum dots, Appl. Phys. Lett. 76 (2000) 137–139.
[31] M. Stroscio, M. Dutta, D. Kahn, K.W. Kim, S. Komirenko, Phonons in nanostructures: device applications, Phys. B: Condens. Matter 316–317 (2002) 8–11.
[32] J.S. Blakemore, Solid State Physics, second ed., Cambridge University, England, 1985.
[33] Y.M. Sirenko, M.A. Stroscio, K.W. Kim, Elastic vibrations of microtubules in a fluid, Phys. Rev. E 53 (1996) 1003–1010.